ISSN 1 746-7233, England, UK
World Journal of Modelling and Simulation
Vol. 8 (2012) No. 4, pp. 310-320

Finite Element Modeling for Electric Field and Voltage Distribution along the Polluted Polymeric Insulator

Chinnusamy Muniraj and[1*], Subramaniam Chandrasekar[2]

[1] Department of Electrical and Electronics Engineering, K. S. Rangasamy College of Technology, Tiruchengode 637215, India

[2] Principal Gnanamani College of Engineering, Namakkal 637001, India

(*Received April 20 2011, Accepted March 23 2012*)

Abstract. This paper proposes a new Finite Element Model (FEM) to calculate the electric field and voltage distribution on polymeric insulator. The new model incorporates the real insulator geometrical dimensions, its material properties and self-adaptive two dimensional elements. The 11 kV and 22 kV polymeric insulator models are simulated under clean, polluted and dry band surface conditions using 2D Electrostatic software. The electric field distribution, voltage distribution and heat generated on the surface are investigated in all the surface conditions. The maximum electric filed strength and the place where it occurs has been studied for all the surface conditions. Based on the above investigation, the simulation results have been presented and analyzed for polymeric insulators. The maximum electric field strength value is compared with Boundary Element Model (BEM). The results are in good agreement with the published work.

Keywords: polymeric insulator, finite element method, pollution, electric filed, Voltage distribution

1 Introduction

Composite insulators are widely used in the power system because of their lighter weight, higher mechanical intensity, better antipollution performance and lower maintenance requirements. The 11kv silicon rubber insulator which is used in this work is shown in Figure1.The presence of pollution layer on composite insulator is very frequent near industrial, agricultural and coastal areas. This pollution layer when combined with moisture due to wet weather conditions such as dew, fog or drizzle, becomes conductive and a leakage current flows through it[1, 4]. Due to flow of leakage current dry bands may form on the insulator surface and the distribution of electric field and potential become distorted and flashover may occur[11]. Therefore, it is important to compute the electric field and potential in studying the characteristics and behavior of polluted composite insulators. The electric field distribution of polymeric insulator is different compared to porcelain insulators. Generally the electric field distribution of a composite insulator is more nonlinear than that of a porcelain insulator. The field distribution can be evaluated using numerical techniques, such as, the Boundary Element Method (BEM), the Charge Simulation Method (CSM), the Finite Difference Method (FDM) and the Finite Element Method (FEM). Rasolonjanahary et al. [13] have proposed a new method based on boundary integral equation to calculate the electric field and voltage distribution of polluted insulators. Hartings [8] also conducted a series of experiments to study the AC behaviour of hydrophilic and hydrophobic post insulators during rain. The radial and axial components of the electric field strength along an insulator under dry and rain conditions were measured. El-Kishky and Gorur [5] used a modified Charge Simulation Method for calculating the electric potential and field distribution along AC HV outdoor insulators. Accurate modelling of a non-ceramic insulator could be achieved with a significant reduction in the number of charges used in this

* Corresponding author. *E-mail address*: c.muniraj@gmail.com.

method. C. Volat et al. [15] have determined the potential and electric-field distributions along a typical ceramic extremely-high-voltage post insulator covered with atmospheric ice during a melting period. The results obtained have shown that numerical simulations can be a good alternative to experimental measurements. A. Phillips et al. [2] have studied the electric field distribution around the polymeric insulators with corona rings. For most transmission line applications, the dominant direction of the electric field is along the axis of the insulator. Even though many research papers have been published earlier; there are still many issues to be solved in this problem as all the previous research papers considered only the approximated geometry for calculation of electric field and voltage distribution (EFVD). The FEM is most convenient for a field with many dielectrics, heterogeneous and nonlinear materials, complex fields and a field containing distributed space charges and singular points. It is one of the most successful numerical methods for solving electrostatic field problems because it involves discretization of the domain according to the anticipated value of field distributions[14]. It is also a flexible method that is well suited to problems with complicated geometry[3, 7]. The FEM leads to comparatively simpler techniques for estimating fields at highly curved and thin electrode surfaces with different dielectric materials[6, 9].

Fig. 1. Photograph of 11 kv silicon rubber insulator

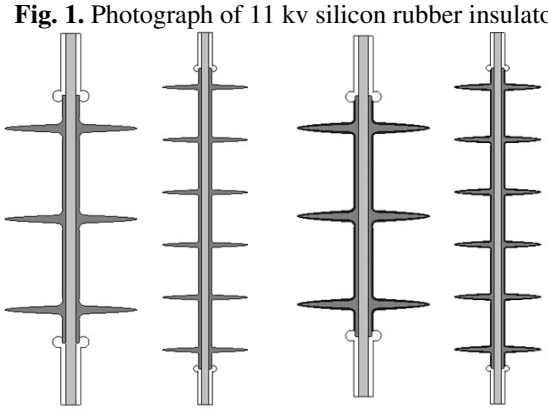

Fig. 2. FEM model of 11kv & 22kv insulator (a) Clean and dry model, (b) uniformly polluted model

In this paper adaptive two dimensional FEM model is developed based on real geometrical dimensions and it is implemented to calculate the electric field and potential distribution of polluted 11kv and 22kv polymeric insulator [PPI]. The main objective of this paper is to study the electric field and potential distribution of clean and dry insulators, uniformly polluted insulators and uniformly polluted insulators with dry band. The above study has been carried out by 2D Electrostatic software. This paper is organized as development of FEM model, Solving FEM, Electric field and potential contours analysis, Calculation of electrical field in different areas on surface of insulator and calculation of heat generated on the surface.

2 FEM model of 11 kv and 22 kv polymeric insulator

Polymeric insulators have four major components: (i) fiber reinforced polymer (FRP) rod; (ii) polymer sheath on the rod; (iii) polymer weather sheds; (iv) metal end fittings. In the present work, insulator made with

silicone rubber polymeric material is considered for simulation Dimensions of the 11 kV and 22 kV silicone rubber insulators used in the simulation study are shown in Tab. 1.

Fig. 2 shows the FEM model of silicone rubber insulators used in the study. This paper investigates the Electric field and voltage distribution [EFVD] of the 11kV and 22 kV polymeric insulators at three different surface conditions such as

Case 1: Dry and clean insulator;

Case 2: Uniform medium pollution layer on the insulator surface;

Case 3: Dry band of 1 cm introduced in the sheath of the uniformly polluted insulator.

Tab. 2 shows the properties of the materials such as relative permittivity, conductivity and thickness/height of pollution layer and dry band used for the FEM modeling of the insulators. The insulator is equipped with metal fittings at both line and ground ends.

Table 1. Geometrical parameter of composite insulators

	11kv	22kv
Total length	276 mm	476 mm
Disc diameter	90 mm	90 mm
No.of Disc	3	6
Creepage distances	323 mm	600 mm

Table 2. Material properties of FEM model

Properties	SIR	FRP core	Pollution layer	Dry band	Air
Relative Permittivity, (ε_r)	4.3	7.2	-	-	1
Conductivity, μ s/cm	0	0	10	0	0
Thickness/Height	-	-	1 mm/-	1 mm/1 cm	-

3 Finite element method of analysis

An easy way to evaluate the electric field distribution is to calculate electric potential distribution initially and then calculate field distribution by subtracting gradient of electric potential distribution from it[3].

This can be written as follows,

$$E = -\nabla V. \tag{1}$$

From Maxwell's equation,

$$\nabla E = \frac{\rho}{\varepsilon}, \tag{2}$$

where ρ is volume charge density, ε is permittivity of dielectric material $(\varepsilon = \varepsilon_0 \varepsilon_r)$, ε_0 is air or space permittivity (8.854×10^{-12}) and ε_r is relative permittivity of dielectric material The Poisson's equation can be obtained by substituting Eq. (1) in Eq. (2)

$$\nabla^2 V = -\frac{\rho}{\varepsilon}. \tag{3}$$

The Laplace's equation can be obtained by making space charge $\rho = 0$,

$$\nabla^2 V = 0. \tag{4}$$

The two dimensional function $F(v)$ in the Cartesian system of coordinates can be written as follows,

$$F(v) = \frac{1}{2}\iint \left[\varepsilon_x \left(\frac{\mathrm{d}v}{\mathrm{d}x}\right)^2 + \varepsilon_y \left(\frac{\mathrm{d}v}{\mathrm{d}y}\right)^2\right] \mathrm{d}x\mathrm{d}y, \tag{5}$$

where ε_x and ε_y are the $x-$ and $y-$ components of the permittivity in the Cartesian system of coordinates and v is the electric potential. In the case of isotropic permittivity distribution ($\varepsilon = \varepsilon_x = \varepsilon_y$), the above equation can be rewritten as,

$$F(v) = \frac{1}{2}\iint \varepsilon \left|\nabla v\right|^2 \mathrm{d}s. \tag{6}$$

If the effect of pollution layer conductivity on the electric field distribution is considered, the complex function $F(v)$ should be taken as

$$\overset{*}{F}(v) = \frac{1}{2}\iint (\sigma + j\omega\varepsilon) \left|\overset{*}{\nabla} v\right|^2 \mathrm{d}s, \tag{7}$$

where ω is angular frequency, σ is conductivity of pollution layer μS/cm, and $\overset{*}{F}(v)$ complex potential function.

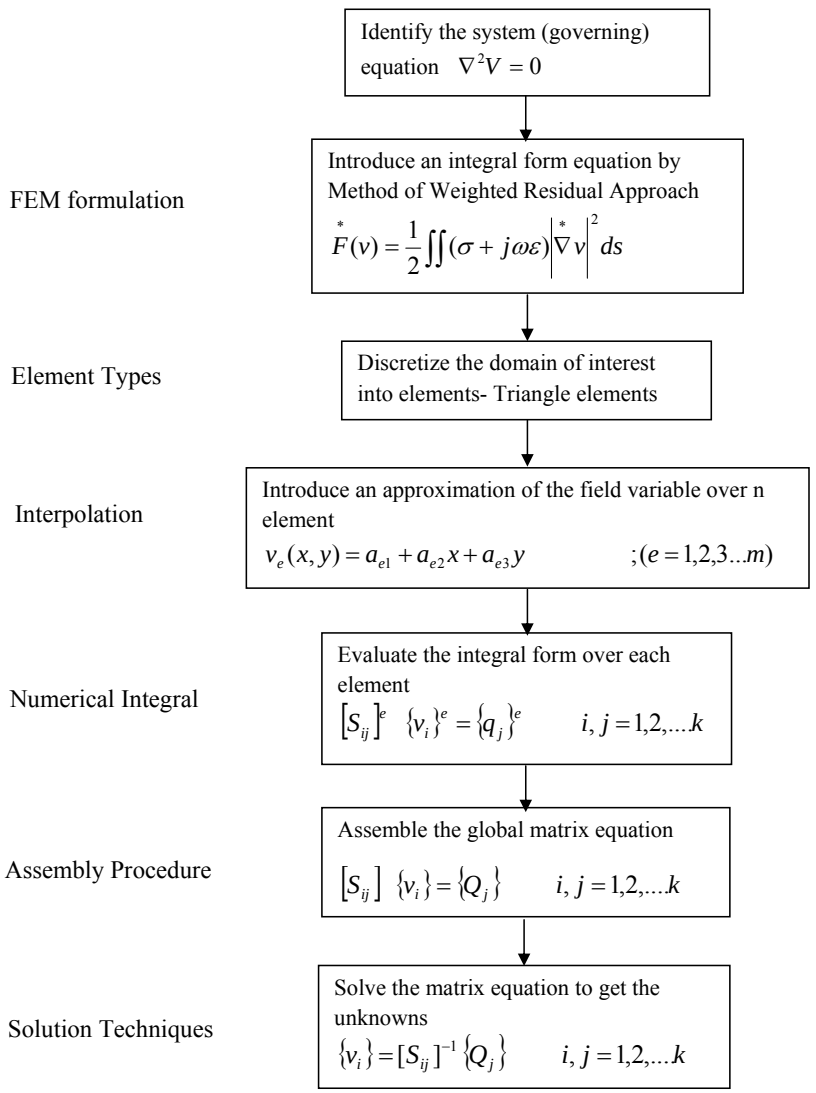

Fig. 3. Flow chart for simulating FEM

Inside each sub domain is assumed a linear dependency of v on x and y, which gives rise to the first order approximation,

$$v_e(x,y) = a_{e1} + a_{e2}x + a_{e3}y, \quad (e = 1, 2, \cdots, m), \tag{8}$$

where $v_e(x,y)$ is the electric potential of any arbitrary point inside each sub-domain, a_{e1}, a_{e2}, a_{e3} are the computational coefficients for a triangle element e, and m is the total number of triangle elements.

The calculation of the electric potential at every node in the total network composed of many triangle elements is carried out by minimizing the function $F(v)$, that is

$$\frac{\partial F(v_i)}{\partial v_i} = 0, \quad i = 1, 2, \cdots, k, \tag{9}$$

where k is the total number of node in the network. The final matrix expression is

$$[S_{ij}]^e [v_i]^e = \{q_j\}^e, \quad i, j = 1, 2, \cdots, k, \tag{10}$$

where $|S_{ij}|$ is the stiffness matrix, $\{v_i\}$ is the unknown potentials vector matrix and $\{q_j\}$ is the free terms matrix vector. The above matrix equation is solved by iterative methods. The computer simulation algorithm flow chart for FEM has shown in Fig. 3.

4 Results and discussion

4.1 Dry and clean insulator

Figure 4a and 4b shows the equi-potential contours and Electric field contours of 11 kV silicone rubber insulator under clean dry surface condition respectively. Similarly Fig. 5 shows the equi-potential contours and Electric field contours of 22 kV silicone rubber insulator under clean dry surface condition respectively. From the figures, as expected, it is noticed that the potential contours and Electric field contours of the clean and dry insulator are without any distortions from high voltage end to the ground end. It is also noticed that the maximum electric field stress is occurring at the high voltage end fitting curvature.

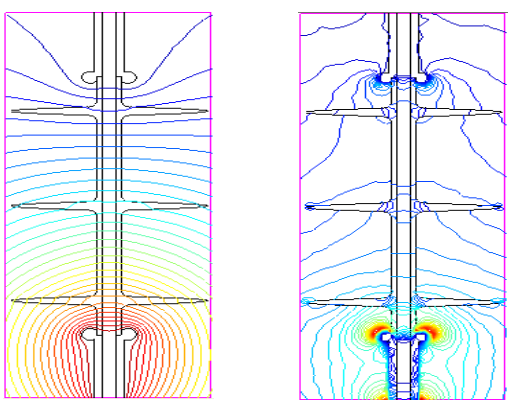

Fig. 4. (a) Equi-potential contours (b) Electric field contours of 11 kV silicone rubber insulator under clean dry surface condition

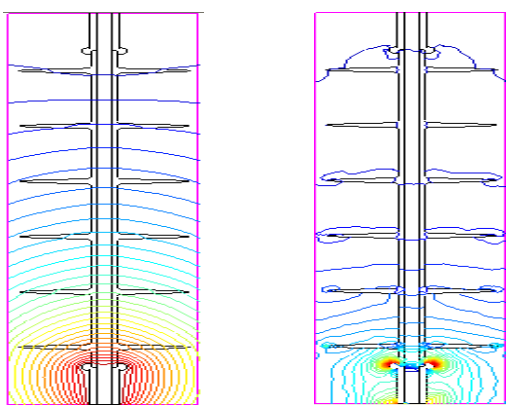

Fig. 5. (a) Equi-potential contours (b) Electric field contours of 22 kV silicone rubber insulator under clean dry surface condition

4.2 Polluted insulator

Fig. 6 shows the equi-potential contours and electric field contours of 11 kV silicone rubber insulator under uniformly, lightly polluted surface condition respectively. Similarly Fig. 7 shows the equi-potential

contours and electric field contours of 22 kV silicone rubber insulator under uniformly, lightly polluted surface condition respectively. In general, it can be observed that the potential and electric field contours of the polluted insulators are significantly distorted over the insulator surface from line end to ground end due to presence of the pollution layer. It is observed that electric field strength is much higher at the junction region between the sheath and the shed than at the middle part of the sheath region. In addition, the electric field contours lines are also concentrated at the tip of the weather sheds to some extent and maximum electrical stress is noticed at the tip of the first shed nearer to high voltage end when compared with other sheds.

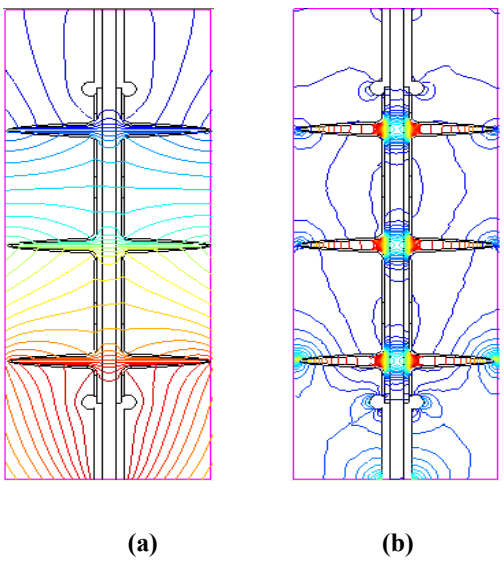

Fig. 6. (a) Equi-potential contours (b) Electric field contours of 11 kV silicone rubber insulator under uniformly, lightly polluted condition

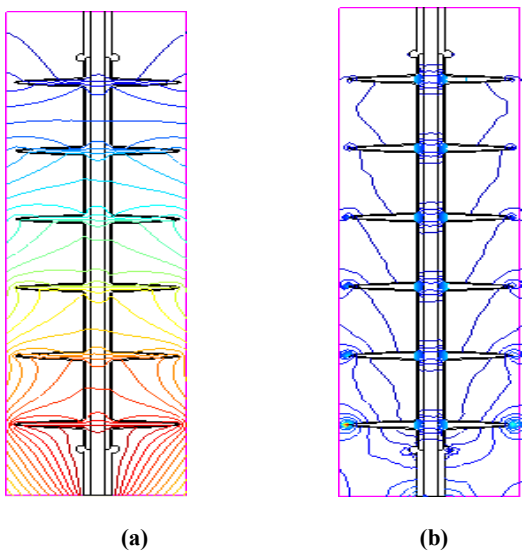

Fig. 7. (a) Equi-potential contours (b) Electric field contours of 22 kV silicone rubber insulator under uniformly, lightly polluted condition

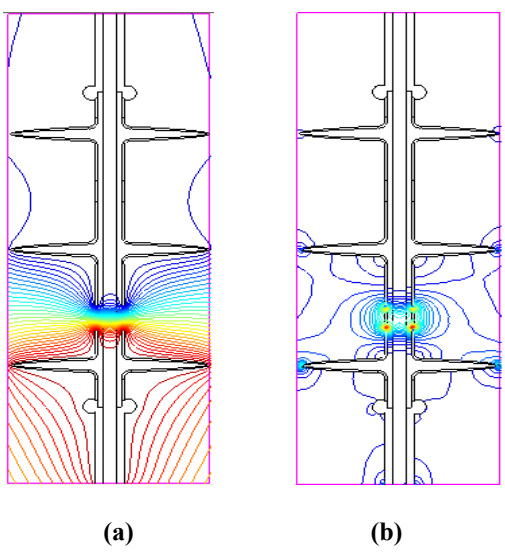

Fig. 8. (a) Equi-potential contours (b) Electric field contours of 11 kV silicone rubber insulator under lightly polluted condition with dry band formation

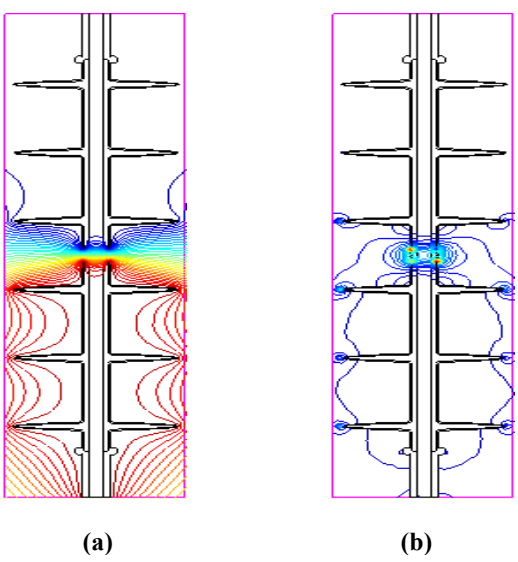

Fig. 9. (a) Equi-potential contours (b) Electric field contours of 22 kV silicone rubber insulator under lightly polluted condition with dry band formation

4.3 Polluted insulator with dry band formation

Fig. 8 shows the equi-potential contours and Electric field contours of 11 kV silicone rubber insulator under uniformly, lightly polluted surface condition with dry band formation respectively. Similarly Figure 9a and 9b shows the equi-potential contours and Electric field contours of 22 kV silicone rubber insulator under uniformly, lightly polluted surface condition with dry band formation respectively. Dry band for the 11 kV insulator is simulated nearer to high voltage end, whereas for 22 kV insulator it is simulated in the middle of the insulator. From the figures, it is observed that the high voltage is shifted to the edge of the dry band located towards the line end and similarly the earth potential is transferred from the ground end fitting to the another edge of dry band. Thus a very high potential is noticed across the dry band.

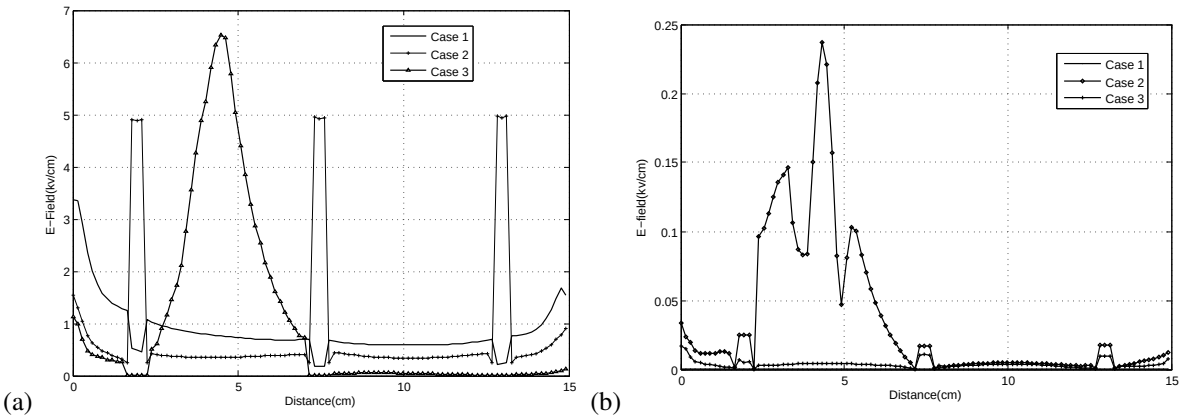

Fig. 10. Electric field distribution of the 11 kV silicone rubber insulator (a) Real part, (b) Imaginary part

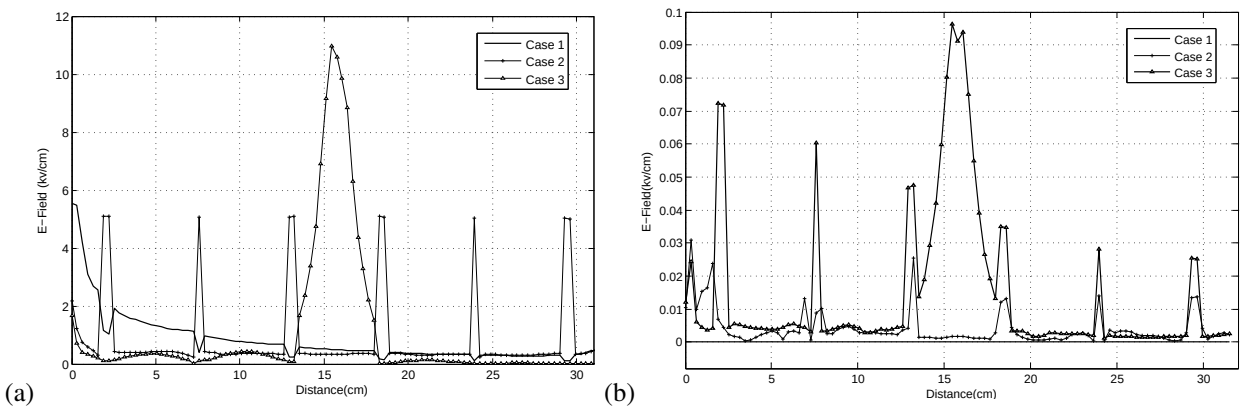

Fig. 11. Electric field distribution of the 22 kV polymeric insulator (a) Real part, (b) Imaginary part

From the electric field contours, it is noticed that the electric field lines are concentrated towards the dry band region and the maximum electric field strength is observed in the dry band region. Since the electric field stress across the dry band exceeds the breakdown stress of air, it leads to the formation of partial arc across the dry band. This partial arc is the root cause for the increase in surface temperature, surface degradation due to thermal stress and finally flashover of the polymeric insulator. In real time situations, the dry band may appear at any place on the surface of the insulator due to the non-uniform leakage current density. Considering this, in the present work, simulation was carried out with dry band at different locations on the surface of the insulator such as nearer to high voltage end, nearer to ground end and at the middle of the insulator. From the above reported simulation results, maximum electric field strength is calculated for both 11 kV and 22 kV insulators at different surface conditions and it is reported in Tab. 3. From the tabulated results, it is observed that the electric field stress is very much enhanced when the dry band is located nearer to the high voltage end for both 11 kV and 22 kV insulators. The FEM modeling results has been compared by Boundary Element Method (BEM). The comparative results has shown in the Tab. 3.

5 Analysis of electric field along the sheath and tip of sheds of insulator

The real and imaginary components of Electric field strength along the sheath surface of the insulator were also calculated for three different surface conditions (refer case1, 2 and 3). The calculation path (the line A-B shown in Fig. 1 (a)) is 4mm away from the surface of the sheath and starts from the point 0.2 mm above the line end metal fitting. Fig. 10 shows the real and imaginary parts of electric field distribution along the sheath surface of 11 kV insulator respectively. Corresponding results for 22 kV insulator are shown in Fig. 11. It is observed that the EFVD along the insulator under uniform pollution condition is completely different from the dry and clean insulator. Under polluted conditions, electric field strength in the shed section is larger than middle of sheath section. In the case of dry band formation conditions, electric field is much higher in the dry band region than other regions. It is also noticed that the imaginary part of EFVD is absent under clean dry surface conditions, whereas it is present under polluted conditions and it may be attributed to the flow of leakage current under polluted conditions.

Table 3. The maximum Electric field Strength [MEFS]

	MEFS (kv/cm)			
	11kv		22kv	
	FEM	BEM	FEM	BEM
Dry and clean	3.82	3.21	5.92	5.05
Uniform pollution	5.15	5.05	16.29	15.28
uniform pollution with dry band at middle	-	-	43.48	41.48
uniform pollution with dry band at near H.V end	31.3	30.3	54.58	50.58
uniform pollution with dry band at near to L.V end	24.61	23.41	50.48	48.48

It is important to understand the electric field at the tip of the weather sheds under polluted conditions, because electric field stress enhancement also occurs at the small curvature of the shed under polluted conditions. Fig. 12 shows the electric field evaluated at the tip of the weather sheds of 11 kV and 22 kV insulators under polluted conditions. It can be seen that the shed very near to the H.V end is subjected to maximum stress under polluted conditions. It is also observed that the electric field stress at the shed tips is higher than the stress at middle part of sheath region.

6 Analysis of voltage distribution along the sheath of insulator

The potential distribution along the sheath surface is shown in Fig. 13 and 14. Real part of potential in dry and clean conditions is linear between two ends, and there is no imaginary part. In other two cases the potential distribution curve was different then clean and dry conditions. In uniformly polluted case real part of the potential is getting non linear and distribution curve is away from the clean and dry condition and imaginary part is presented in the negative side. In the dry band conditions the real part of the potential is divided in two parts one is maximum value (11k and 22kv) and the other is minimum value (0 kv) and positive and negative imaginary part also presented.

7 Evaluation of the degree of uniformity

The degree of uniformity (η) is a measure of the uniformity of a field and it is defined as [12],

$$\eta = \frac{V}{d * E_{\max}}, \tag{11}$$

where $E_{\max}$ = Maximum Electric field strength, V = Applied voltage.

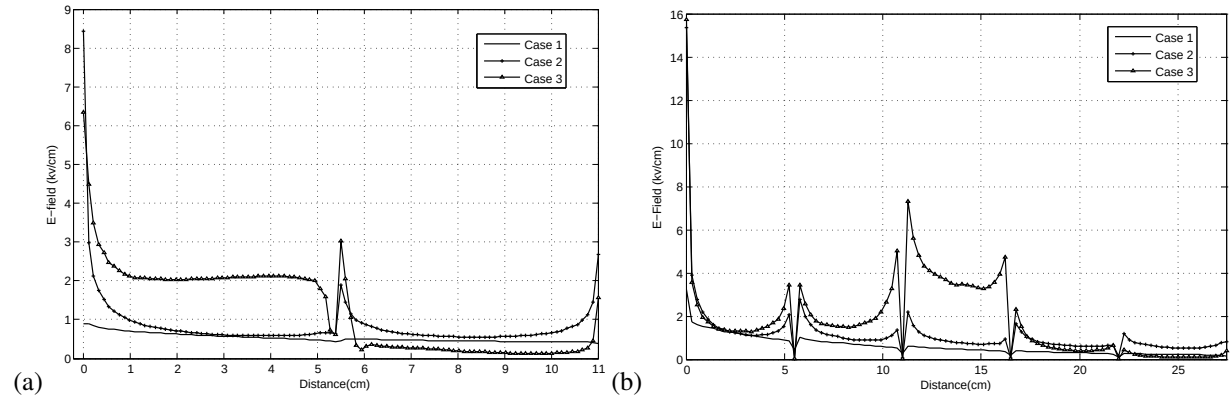

Fig. 12. Electric field distribution of the polymeric insulator at the tip of the shed (a) 11 kV (b) 22 kV

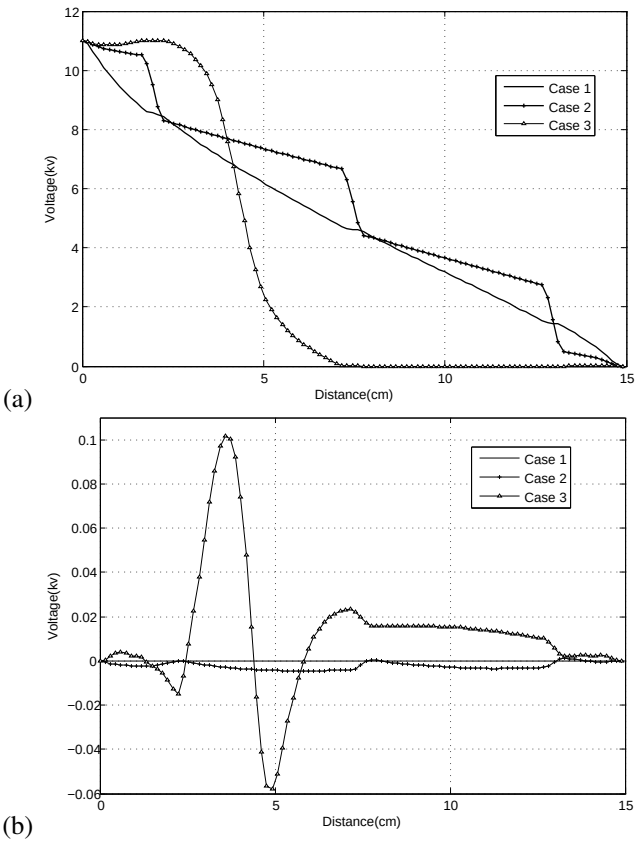

Fig. 13. Voltage distribution of the 11 kV polymeric insulator (a) Real part, (b) Imaginary part

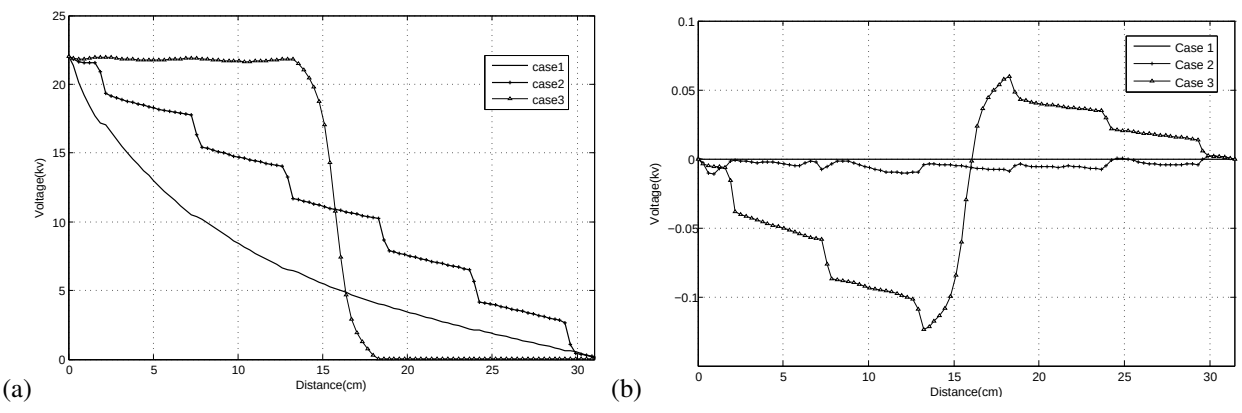

Fig. 14. Voltage distribution of the 22 kV polymeric insulator (a) Real part, (b) Imaginary part

Thus η, a dimensionless quantity enables to make a comparison of the uniformity of fields formed between two electrodes. The degree of uniformity of the electric field is evaluated at different surface conditions of polymeric insulators and it is reported in Tab. 4. As expected, it is observed that under polluted conditions the uniformity is very less when compared with clean and dry conditions. This confirms that the electric field and voltage distribution [EFVD] of polymeric insulator is highly non-linear at wet polluted conditions.

8 Evaluation of the heat generated in the surface of insulator

As reported in the experimental results, the magnitude of leakage current flow during clean and dry surface condition is negligible and therefore the possibility for surface heat generation is very less. Whereas, under polluted conditions, significant amount of leakage current is flowing and it can generate considerable amount of heat on the surface of insulator. This heat plays a major role in the formation of dry bands over the insulator surface and therefore which will lead to partial arcing and surface degradation of the polymeric insulator. When the arcing continues and elongates, it will result in the flashover.

Therefore it becomes necessary to understand the amount of heat generated in polymeric insulators in order to improve its thermal resistance during manufacturing process. The heat generated by the A.C is given by [3, 10, 12]

$$W_{ac} = \frac{E^2 f \varepsilon_r \tan\delta}{1.8 * 10^{12}}, \tag{12}$$

where E is from E_{max} and $f = 50$ Hz, the $\tan\delta$ for silicone rubber is 0.006. Using the above formula, the heat generated in the surface of the insulator was evaluated and reported in Tab. 5. It is observed that more heat is generated when the dry band formation is nearer to high voltage end and therefore the possibility of surface degradation of polymeric insulator nearer to high voltage end is more when compared with other portions.

Table 4. The degree of uniformity

	The degree of uniformity (η)	
	11 kV	22 kV
Dry and clean	0.192	0.116
Uniform pollution	0.142	0.052
Uniform pollution with dry band at middle	-	0.016
Uniform pollution with dry band near H.V end	0.023	0.013
Uniform pollution with dry band near to L.V end	0.03	0.014

Table 5. Heat generated in polymeric insulator

	Heat Generated Wac (mW/cm^3)	
	11 kV	22 kV
Dry and clean	0.01045	0.02511
Uniform pollution	0.019	0.19
Uniform pollution with dry band at middle	-	1.354
Uniform pollution with dry band near H.V end	0.7021	2.134
Uniform pollution with dry band near to L.V end	0.434	1.826

9 Conclusion

Electric field and voltage distribution (EFPD) along polluted composite insulators have been analyzed in this paper. This analysis showed that the effect of the medium uniform pollution layer on a composite insulator

is to linearise the potential distribution along the length of the insulator. The potential distribution along the insulator surface was dividing into two levels as maximum towards HV end and minimum towards LV end by the presence of dry band. Maximum electric field stress can occur at the portion which has a small radius of curvature. The computation of the electric field on the insulator surface confirmed that the spike in electric field distribution created by dry band region was sufficient to initiate an arc along the insulator surface. The electric field along the surface has been largely enhanced and uniformity has been reduced due to the presence of pollution layer and dry band. The heat generated on the insulator surface indicated that pollution layer and dry band can create thermal breakdown. The proposed model with minor modification and new material properties can be used to analysis electric field redistribution due to different ageing of polymeric insulators.

References

[1] Walyo et al. Study on leakage current waveforms of porcelain insulator due to various artificial pollutants. *International Journal of Mathematical, Physical and Engineering Sciences*, 2007, **2**(1): 27–32.

[2] J. Andrew. Electric fields on ac composite transmission line insulators. *IEEE Transactions on Power Delivery*, 2008, **23**(2): 823–830.

[3] R. Arora, W. Mosch. High voltage insulation engineering. *New age internal (p) Limited*.

[4] S. Chandrasekar, R. Sarathi, M. Danikas. Analysis of surface degradation of silicone rubber insulation due to tracking under different voltage profiles. *International Journal of Electrical Engineering*, 2006. Springer.

[5] H. El-Kishky, R. Gorur. Electric potential and field computation along ac hvinsulators. *IEEE Transactions on Dielectrics and Electrical Insulation*, 1994, **1**(6): 982–990.

[6] Y. Gu, J. Li. Finite element analysis of the instep fatigue trauma in the high-heeled gait. *World Journal of Modelling and Simulation*, 2005, **1**(2): 117–122.

[7] Z. Guan, L. Wang, et al. Electric field analysis of water drop corona. *IEEE Transactions on power delivery*, 2005, **20**(2): 964–969.

[8] R. Hartings. Electric fields along a post insulator: Ac-measurements and calculations. *IEEE Transactions on Power Delivery*, 1994, **9**(2): 912–918.

[9] Y. Liu, C. Yu1, et al. 3d fe model reconstruction and numerical simulation of airflow for the upper airway. *World Journal of Modelling and Simulation*, 2006, **2**(3): 190–195.

[10] C. Muniraj, S. Chandrasekar. Computation of electric field and potential distribution around a polluted composite insulator by finite-element method. **in:** *Proceedings of the 1st International Electrical Energy systems & power Electronics in Emerging Economics Conference*, **1**, Chennai, India, 2009, 247–258.

[11] C. Muniraj, S. Chandrasekar. Investigation of the arc activity on high-voltage polymeric insulators. *International Journal of Power and Energy Systems*, 2011, **31**(2): 01–08. Octapress.

[12] M. Naidu, V. Kamaraju. High voltage engineering. *Tata McGraw-Hill Publishing Company limited*, 1995.

[13] J. Rasalonjanahary, L. Krahenbuhl, A. Nicolas. Computation of electric fields and potential on polluted insulators using a boundary element method. *IEEE Transportation On Magnetics*, 1992, **28**(2): 1473–1476.

[14] W. Sima, Q. Yang, et al. Potential and electric-field calculation along an ice-covered composite insulator with finite-element method. **in:** *IEE Proceedings-generation Transmission and Distribution*, *3*, **153**, 2006, 343–349.

[15] C. Volat, M. Farzaneh. Three-dimensional modeling of potential and electric-field distributions along an ehv ceramic post insulator covered with ice-part i:simulations of a melting period. *IEEE Transactions on Power Delivery*, 2005, **20**(3): 2006–2013.